

Electronic Supplementary Information

Directional migration propensity of calf thymus DNA in gradient of metal ions

Shikha, Ekta Shandilya, Priyanka, Subhabrata Maiti*

Department of Chemical Sciences, Indian Institute of Science Education and Research (IISER)
Mohali, Knowledge City, Manauli 140306, India.

*E-mail: smaiti@iisermohali.ac.in

Table of Content

A. Material and Methods.....	S2
B. Melting Temperature study.....	S4
C. DNA-metal ion binding constant	S5
D. Circular Dichroism	S6
E. Atomic Force Microscopy.....	S7
F. Fluorescence and Optical Microscopy.....	S10
G. Microfluidics study.....	S12
H. Theoretical modeling for chemotactic drift.....	S18
I. Coffee ring effect.....	S23
J. References	S32

A. Material and Methods

All commercially available reagents were used without further purification. Deoxyribonucleic acid (DNA) of calf thymus; Acridine Orange (AO); Carboxylate-modified polystyrene latex beads were procured from Sigma-Aldrich. Agarose (low EEO, Molecular biology), Potassium Nitrate (KNO_3) were obtained from HiMedia. Sodium Nitrate (NaNO_3); Magnesium Nitrate ($\text{Mg}(\text{NO}_3)_2$) from Molychem. Zinc Nitrate ($\text{Zn}(\text{NO}_3)_2$); Copper Nitrate ($\text{Cu}(\text{NO}_3)_2$); Calcium Nitrate ($\text{Ca}(\text{NO}_3)_2$); Ethidium Bromide(EtBr) were purchased from Sisco Research Laboratory, India (SRL) .

Stock solution of acridine orange was prepared using UV-visible spectroscopy having molar extinction coefficient ϵ_{430} (Acridine Orange) = $27000 \text{ M}^{-1}\text{cm}^{-1}$ using a Varian Cary 60 (Agilent Technologies) spectrophotometer. The total volume in the cuvette was fixed at 1 mL, and a cuvette of path length 1 cm was used for the entire study. All the measurements have been performed at 25 °C.

Circular dichroism (CD) measurements were performed using a Biologic spectrophotometer (Science Instruments) with a 1 mm path length quartz cell. The concentration of CT-DNA used for the CD measurement was 30 $\mu\text{g}/\text{mL}$ and 1 mM for metal ions in a 5 mM Tris-HCl (pH=7) buffer. The spectra were recorded over a scan range of 220–360 nm.

Melting temperature measurements were performed using a Cary-Eclipse 3500 (Agilent Technologies). The concentration of CT-DNA and metal ions used for the measurement was 20 $\mu\text{g}/\text{ml}$ and 1 mM respectively in a 5 mM Tris-HCl (pH=7) buffer.

The dynamic light scattering (DLS) data was recorded on a Horiba Scientific Nanoparticle Analyzer SZ-100 V2 fitted with a 10 mW, 532.8 nm laser with a scattering angle of 90°. Zeta potential was measured for 20 $\mu\text{g}/\text{mL}$ CT-DNA and 1 mM metal ions in 5mM tris-HCl Buffer at 25°C. For each sample five repeated measurements after every 10 sec were recorded. To measure the size, a 50 $\mu\text{g}/\text{ml}$ CT-DNA and 1mM metal ions sample in 5mM tris-HCl buffer were taken in a cuvette and measured at fixed temperature of 25 °C. For each sample ten repeated measurements after every 10 sec were performed.

Microfluidics studies were performed using a syringe pump (World Precision Instruments) and microfluidics channels from Venadelta made up of acrylic plastic material was used. 20 $\mu\text{g}/\text{mL}$ CT-DNA and 10 μM AO in 5mM tris-HCl Buffer (pH=7) were injected through top inlet and 1mM metal ions in 5mM tris-HCl Buffer (pH=7) was injected from bottom inlet using syringe pump.

Similarly, the chemotaxis experiment was performed using a 3-inlet-1-outlet channel procured from ChipShop. A solution containing 20 $\mu\text{g}/\text{mL}$ of CT-DNA and 10 μM of AO prepared in buffer was injected through the middle inlet, and 1mM metal ions solution prepared in 5 mM buffer solution was injected from the top and bottom inlet, respectively.

For coffee -ring experiment, 5 μl of solution containing 20 $\mu\text{g}/\text{ml}$ CT-DNA and 10 μM of AO was added over a glass slide, and 1mM of Ca^{2+} was added from one side of a drop and 1mM of Cu^{2+}

was added from the opposite side of the droplet using a syringe pump with a speed of 0.36 ml/hr for 5 seconds (Figure S23). After drying the drop it was analyzed under the optical microscope. Similarly this experiment was done using 0.025% carboxylate modified polystyrene beads in place of Acridine orange.

The optical and fluorescence microscopic images were collected using a Zeiss Axis Observer 7 microscope having AxioCam 503 Mono 3 Mega pixels with ZEN 2 software.

We have used imageJ software for calculation of the fluorescence intensity of the microscopic images, both for microfluidic and coffee ring intensity pattern determination.

For Atomic Force Microscopy (AFM), CT-DNA metal ions sample (DNA concentration was 30 $\mu\text{g}/\text{mL}$ and metal ions concentration were 1mM) were prepared in a 5mM Tris-HCl (pH=7) buffer, after that 10 μL of sample was deposited on a clean surface of mica sheet and incubated for 15-20 min. The mica sheet was washed with 300 μL milli Q water to remove excess salts and non-absorbed material, and then dried with N_2 (g). Innova atomic force microscope (Bruker) operating in tapping mode was used for imaging. Imaging was performed using a silicon Tip on a cantilever (Bruker) and Gwyddion software was used to analyze the AFM images.

For gel electrophoresis, 1.5% (0.75 g in 50 ml) agarose gel with EtBr (0.5 $\mu\text{g}/\text{ml}$) was prepared in TBE (Tris-Borate EDTA) buffer. TBE buffer was used as running buffer and the gel was run for 30 min at 110 V. Images were collected using a Bio Rad gel doc.

B. Melting Temperature study

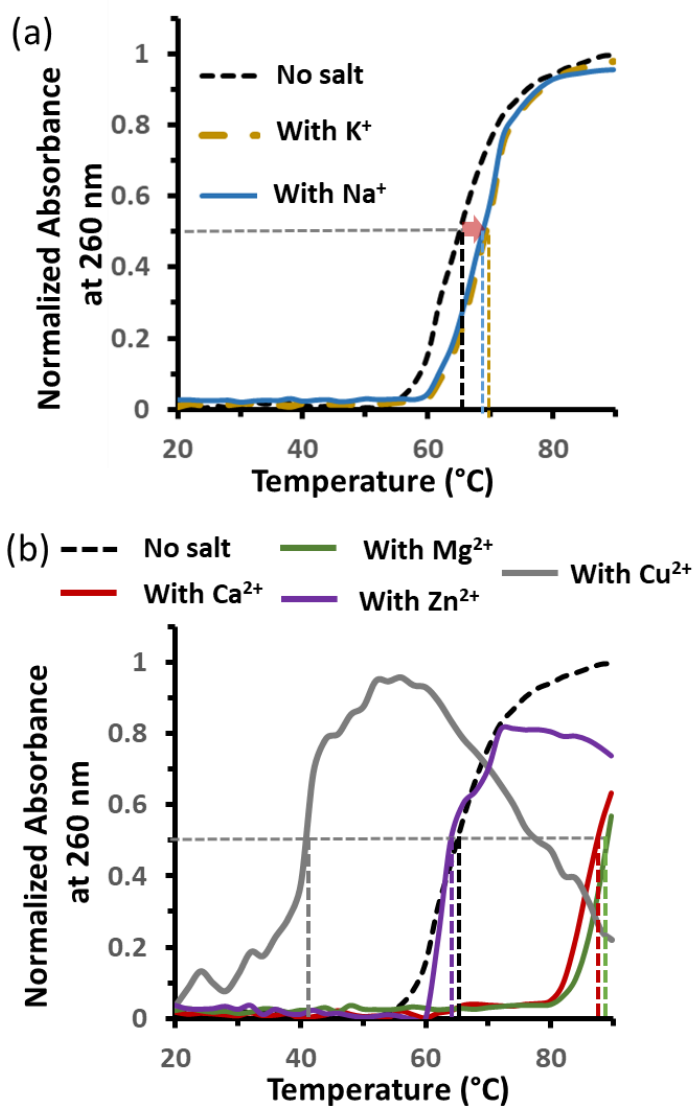


Fig. S1. Normalized absorbance value of CT-DNA at 260 nm as a function of temperature from 20 °C -90 °C in absence and presence of (a) Na⁺ and K⁺ and (b) Mg²⁺, Ca²⁺, Zn²⁺ and Cu²⁺. The dashed line at half of the total absorbance used as a guideline to show the shift in melting temperature of CT-DNA in presence of salts. Black dashed line showed melting curve of only CT-DNA. Experimental condition: [CT-DNA] = 20 µg/ml; [salt] = 1 mM; pH = 7, Tris buffer (5 mM).

C. DNA-metal ion binding constant

Table S1. Binding constant between DNA and metal ions (reference 10 of the main manuscript) at room temp (25 °C).

Metal ions	Binding Constant (M^{-1})
Na⁺	8.6×10^2
Ca²⁺	4.8×10^5
Mg²⁺	3.2×10^5
Cu²⁺	8.0×10^6
Zn²⁺	1.2×10^5

D. Circular Dichroism

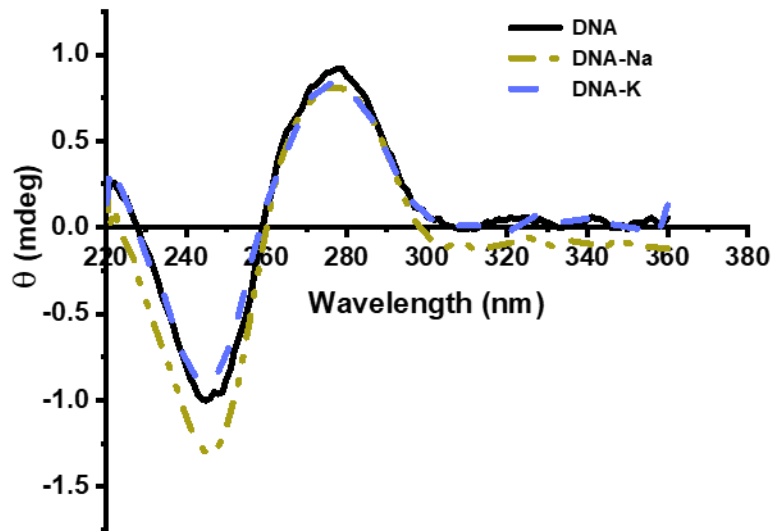


Fig. S2. CD spectra of CT-DNA in absence and presence of monovalent ionic salt of Na^+ and K^+ at 1 mM concentration [CT-DNA] = 30 $\mu\text{g/ml}$.

E. Atomic Force Microscopy

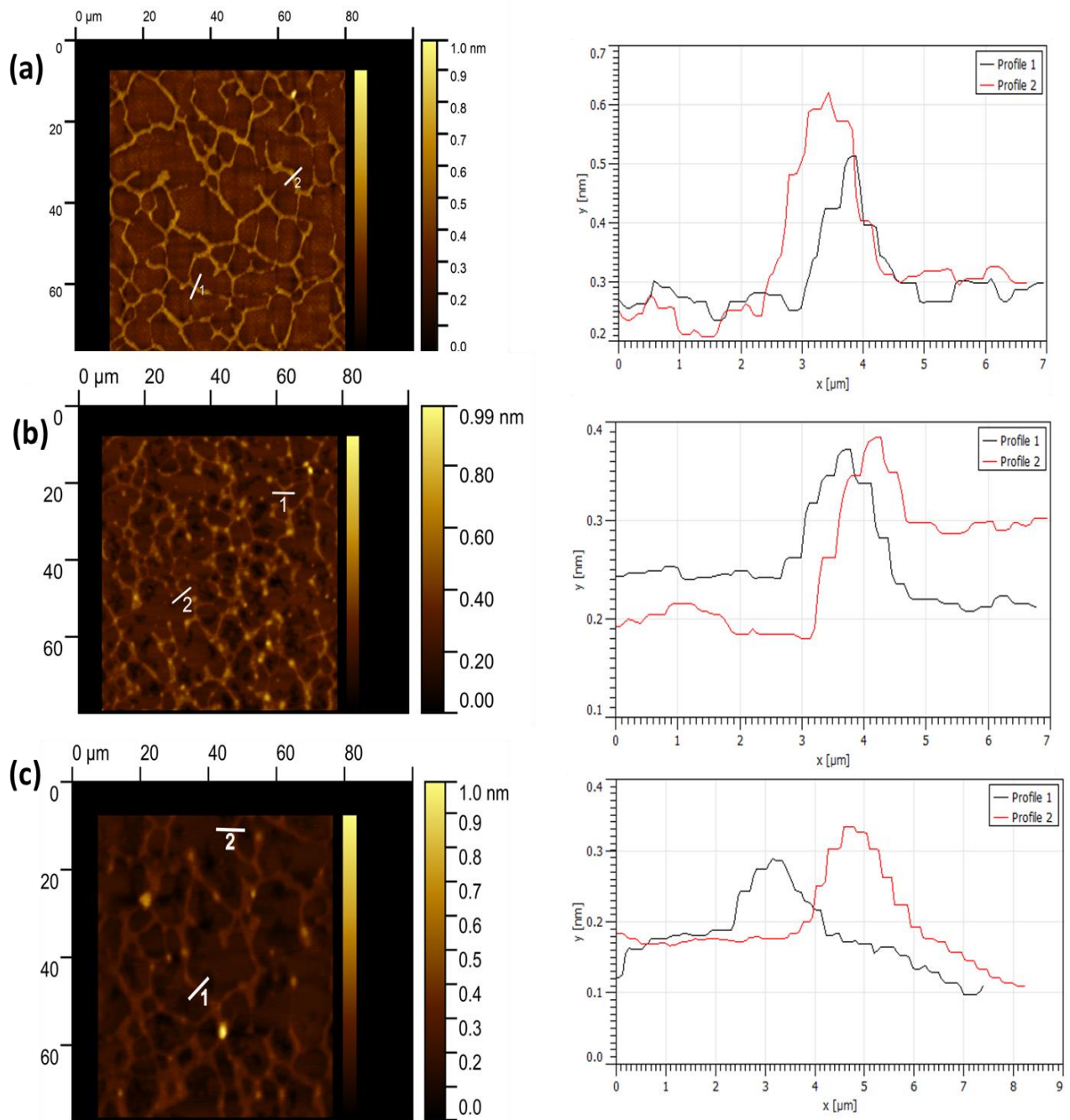


Fig. S3. AFM images of CT-DNA in presence of metal ions (a) Only CT-DNA (b) CT-DNA & Na⁺ (c) CT-DNA and K⁺ Experimental Condition: [CT-DNA]= 30 $\mu\text{g/ml}$, [Na⁺] = [K⁺] = 1mM, Tris-HCl buffer, pH=7, 5mM at 25°C.

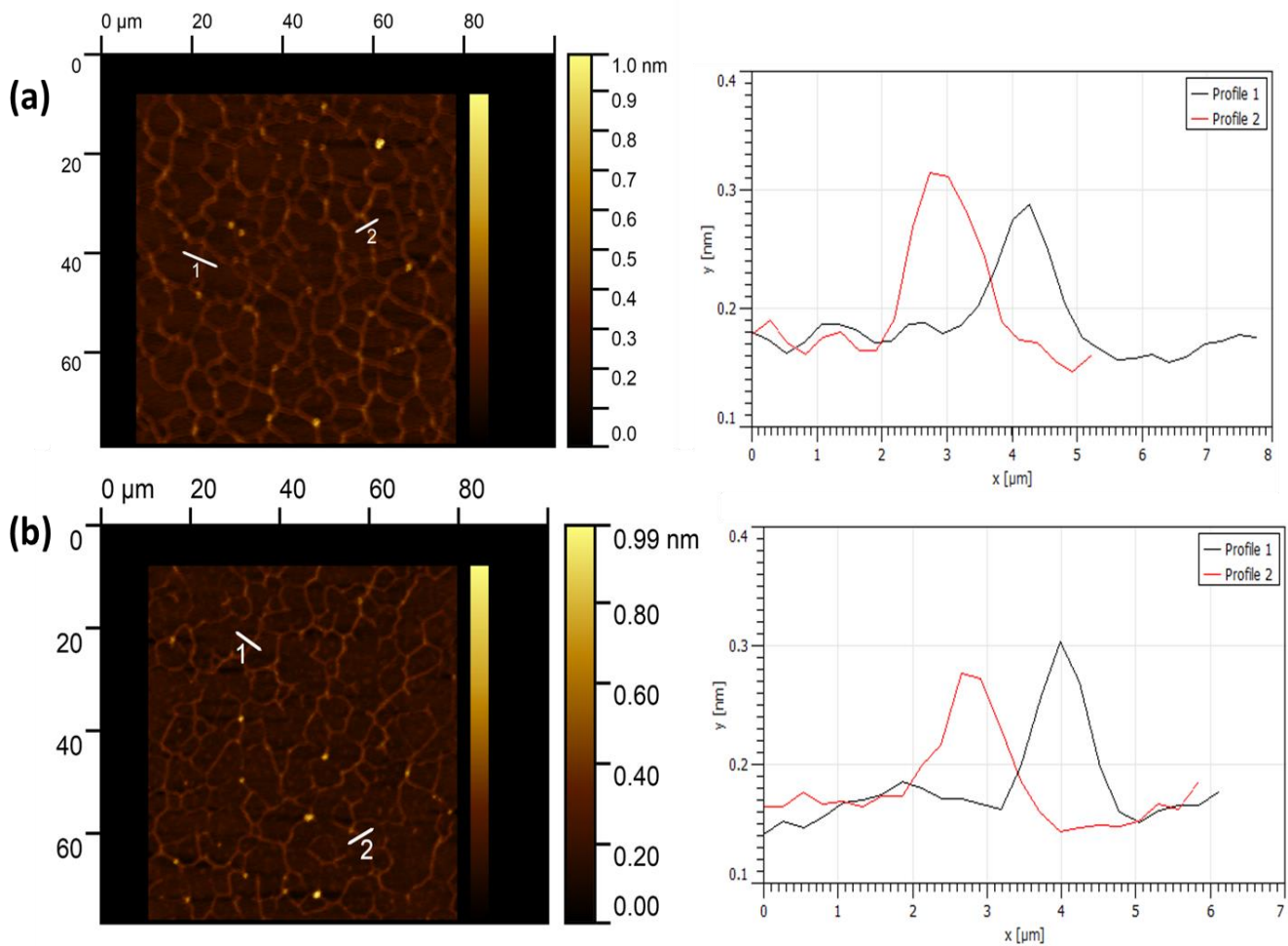


Fig. S4. AFM images of CT-DNA in presence of metal ions (a) CT-DNA and Ca^{2+} (b) CT-DNA and Mg^{2+} . Experimental Condition: [CT-DNA]= 30 $\mu\text{g}/\text{ml}$, [Ca^{2+}] = [Mg^{2+}] =1 mM, Tris-HCl buffer (pH = 7, 5 mM) at 25°C.

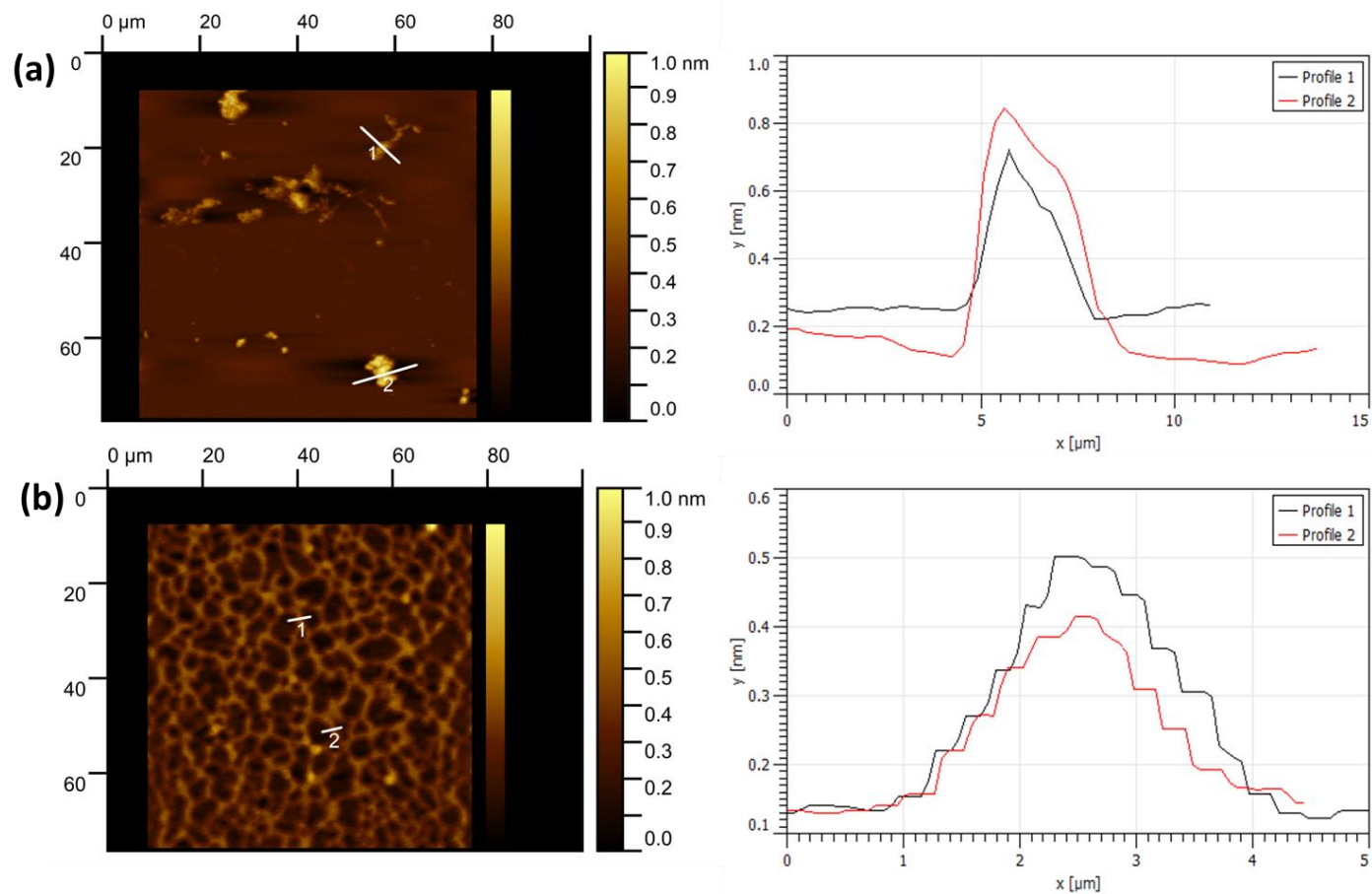


Fig. S5. AFM images of CT-DNA in presence of metal ions (a) CT-DNA and Cu^{2+} (b) CT-DNA and Zn^{2+} Experimental Condition: $[\text{CT-DNA}] = 30 \mu\text{g/ml}$, $[\text{Cu}^{2+}] = [\text{Zn}^{2+}] = 1\text{mM}$, Tris-HCl buffer pH=7, 5mM at 25°C .

F. Optical and Fluorescence microscopy

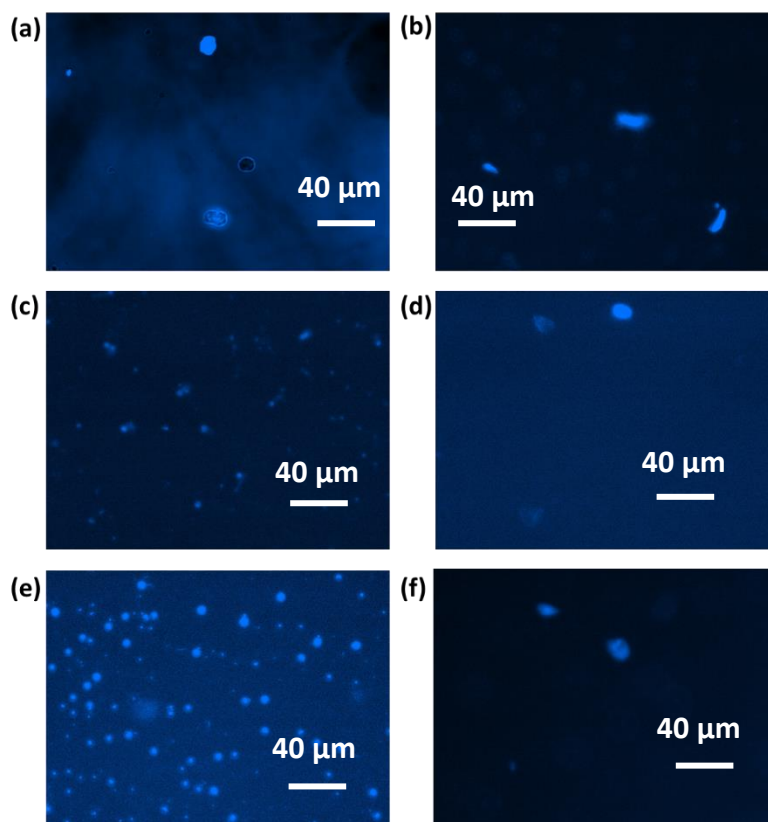


Fig. S6. Fluorescence microscopic images of CT-DNA in presence of metal ions (a) DNA-Na⁺ (b) DNA-K⁺ (c) DNA-Ca²⁺ (d) DNA-Mg²⁺ (e) DNA-Cu²⁺ (f) DNA-Zn²⁺ Experimental Condition: [CT-DNA] = 20 μg/ml, [AO] = 10 μM, [Metal ions] = 1 mM, Tris-HCl buffer pH = 7, 5 mM at 25°C. Only in case of Cu²⁺, many structures of almost similar sized has been observed, suggesting larger condensed DNA structure formed.

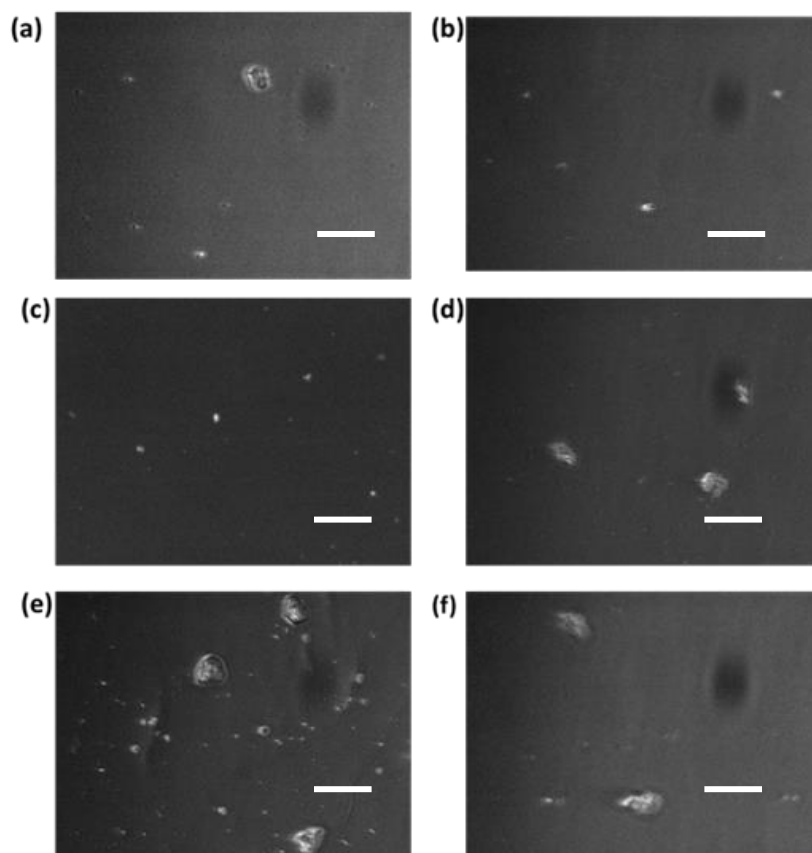


Fig. S7. Optical microscopic images of CT-DNA in presence of metal ions (a) DNA- Na^+ (b) DNA- K^+ (c) DNA- Ca^{2+} (d) DNA- Mg^{2+} (e) DNA- Cu^{2+} (f) DNA- Zn^{2+} Experimental Condition: [CT-DNA]= 20 $\mu\text{g/ml}$, [Metal ions] = 1 mM, Tris-HCl buffer pH = 7, 5 mM at 25°C. Only in case of Cu^{2+} , many structures of almost similar sized has been observed, suggesting larger condensed DNA structure formed. **Scale bar of each image is 40 μm .**

G. Microfluidics study

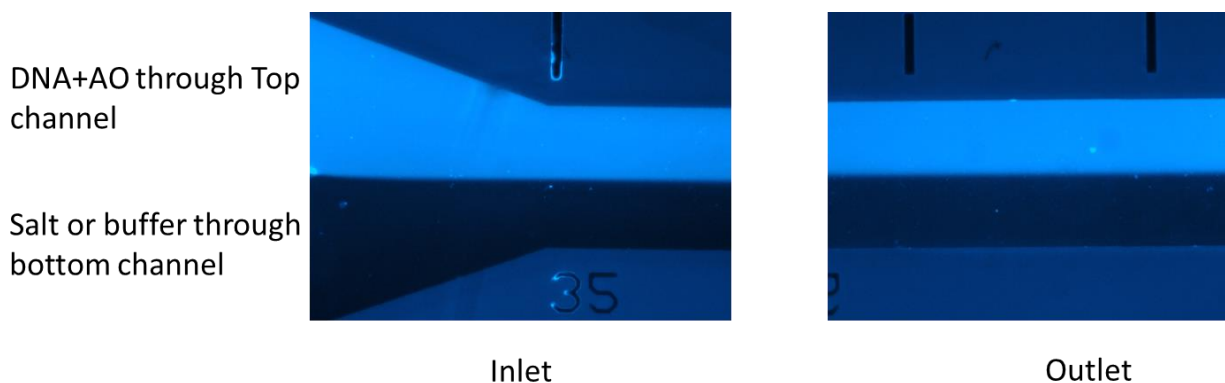


Fig. S8. Typical Fluorescence microscopic images of 2-inlet and 1-outlet of the microfluidics channel with a flow rate of 0.3 ml/hr where 20 $\mu\text{g/ml}$ CT-DNA and 10 μM of AO in 5 mM tris-HCl buffer (pH=7) was injected from the top inlet and through bottom inlet 5mM tris-HCl buffer (pH=7), showing no such deviation only DNA.

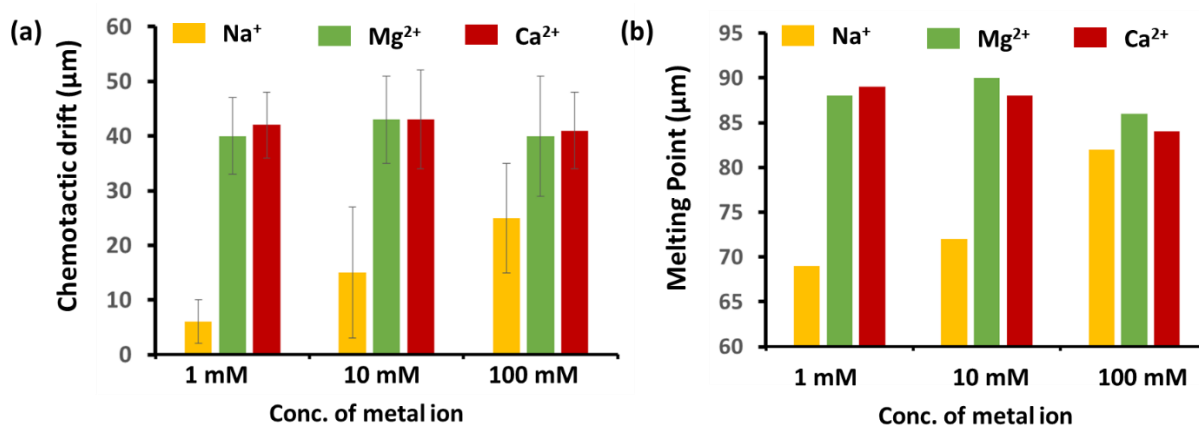


Fig. S9. (a) Measured drift of CT-DNA based on fluorescence intensity calculation towards metal ion side in the experimental set up as denoted in Fig. 3a and S8. Here, different concentration (1, 10 or 100 mM) of Na^+ , Mg^{2+} or Ca^{2+} with NO_3^- as counter ion passed through the bottom inlet and CT-DNA through top. (no. of experiment performed = 3) (b) Melting point of CT-DNA in presence of different concentration of metal ions (Na^+ , Mg^{2+} , Ca^{2+}). [CT-DNA] = 20 $\mu\text{g/ml}$.

Table S2. Zeta potential of CT-DNA in absence and presence of different concentration of metal ions (in all cases nitrate was used as anion).

system [Metal ion]	CT-DNA only	CT-DNA + Na ⁺	CT-DNA + Mg ²⁺	CT-DNA + Ca ²⁺	CT-DNA + Cu ²⁺
0 mM	-48 ± 4 mV	-48 ± 4 mV	-48 ± 4 mV	-48 ± 4 mV	-48 ± 4 mV
1 mM	-	-46 ± 3 mV	-22 ± 4.5 mV	- 26 ± 3.2 mV	-15 ± 3 mV
10 mM	-	-31 ± 4 mV	-14 ± 3 mV	- 13 ± 3.8 mV	-4 ± 2.8 mV
100 mM	-	-15 ± 3 mV	-10 ± 2.5 mV	-9 ± 3 mV	-

Here, we found CT-DNA drift towards metal ion increased with metal ion concentration only for Na⁺ and also it correlated with the melting point increase of CT-DNA. The binding of Na⁺ with CT-DNA increased with increasing concentration and that is reflected in the sharp decrease of negative zeta potential value of CT-DNA as well (Table S2). In fact, overall, the CT-DNA drift correlated with their stability in presence of the metal ion as found from their melting point value. Herein, we were not able to check the CT-DNA drift in presence of Cu²⁺ ion gradient at even 10 mM concentration, as it formed larger visible cluster. The zeta potential of CT-DNA-Cu²⁺ cluster is also low only -4±2.8 mV, suggesting precipitation forming tendency of it. It actually hampers the flow inside the microfluidic channel and thus reliable data was not obtained.

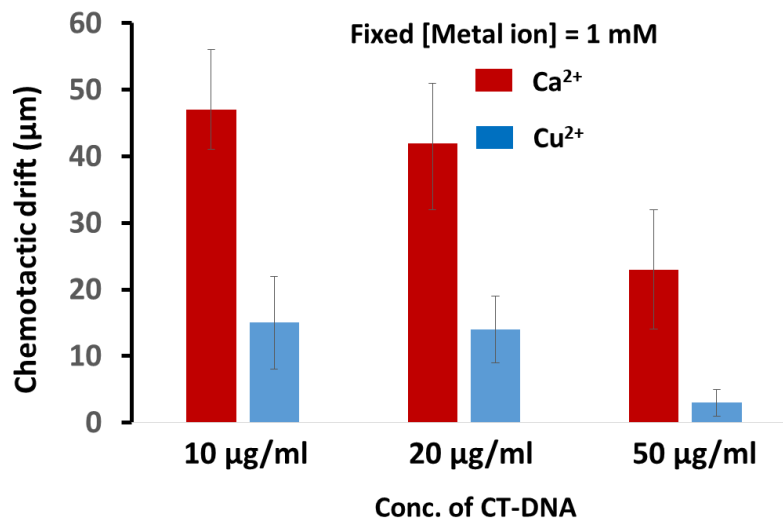


Fig. S10. Measured drift of CT-DNA based on fluorescence intensity calculation towards metal ion side in the experimental set up as denoted in Fig. 3a and S8. Here, fixed concentration (1 mM) of Cu²⁺ or Ca²⁺ with NO₃⁻ as counter ion passed through the bottom inlet and different concentration of CT-DNA (10, 20 and 50 µg/ml) through top. Error bar is the average of triplicate experiment.

We have chosen this study with Ca²⁺ and Cu²⁺ ion gradient as these ions have the maximum and minimum effect over phoretic drift of CT-DNA from our previous study. At high concentration (50 µg/ml) of CT-DNA, low drift is probably due to lesser change in overall CT-DNA property with only 1 mM of ions. However, the trend remains similar as Ca²⁺ showed higher drift and Cu²⁺ lower.

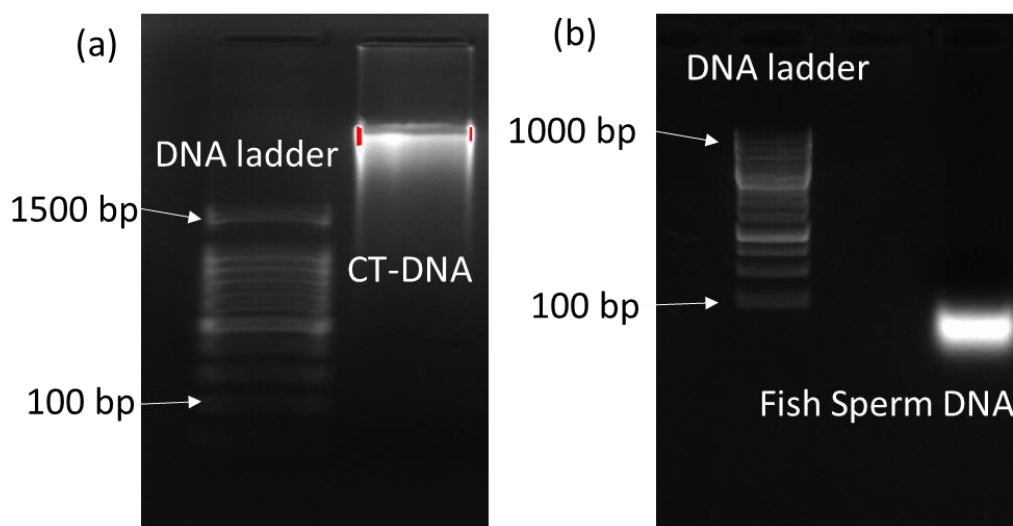


Fig. S11. Agarose gel electrophoresis of CT-DNA and FS-DNA, those were used in our study.

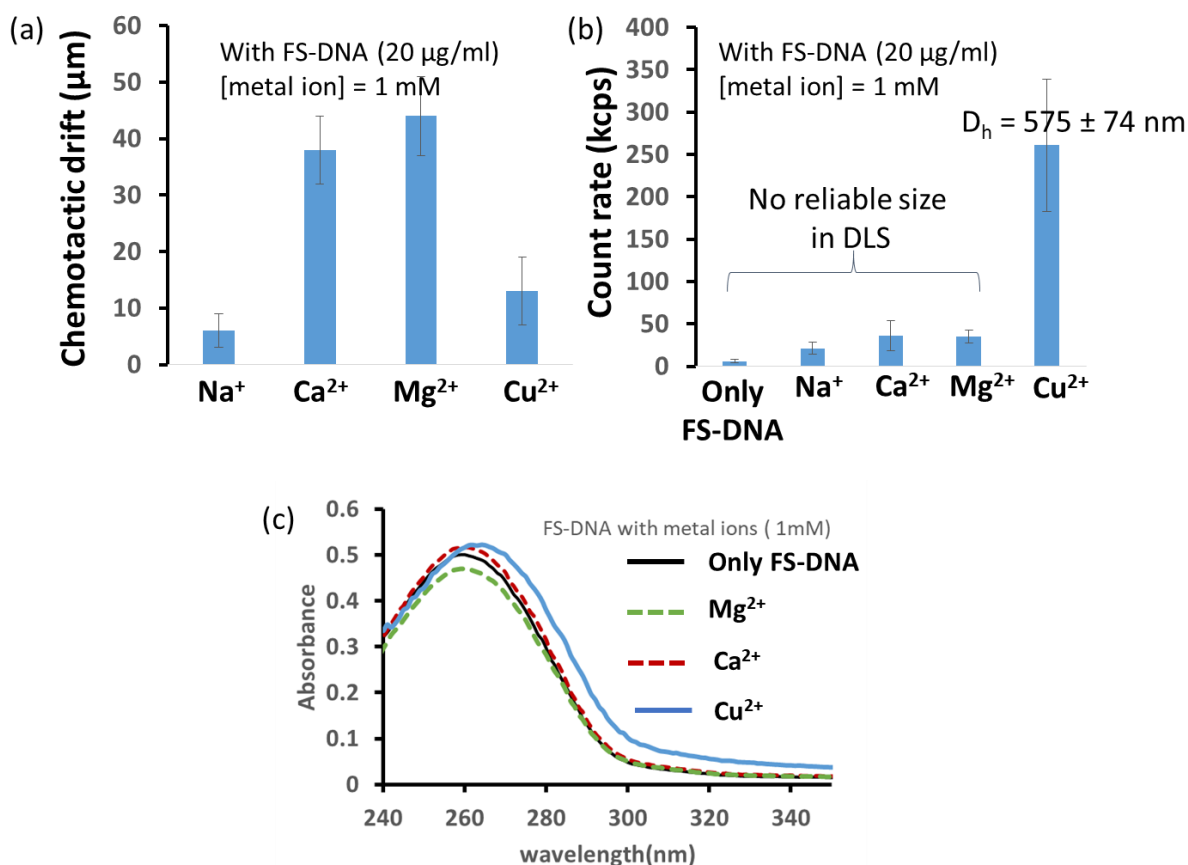


Fig. S12. (a) Measured drift of FS-DNA based on fluorescence intensity calculation towards metal ion side in the experimental set up as denoted in Fig. 3a and S8. Here, fixed concentration (1 mM) of Na⁺, Mg²⁺, Ca²⁺ or Cu²⁺ with NO₃⁻ as counter ion passed through the bottom inlet and FS-DNA with AO through top. (b) Count rate (kcps) of FS-DNA in presence of different metal ions (1 mM) and [CT-DNA] = 20 μg/ml, obtained from DLS measurement. Except Cu²⁺, in all other cases, count rate remains low. It suggests only in presence of Cu²⁺, detectable colloidal aggregate was observed for FS-DNA, which also suggests decreasing of diffusion coefficient of smaller sized FS-DNA in presence of Cu²⁺. (c) UV-vis absorbance spectra of FS-DNA in absence and presence of metal ions. Here also hyperchromicity and a red-shift of 4 nm of FS-DNA absorbance maxima was observed in case of Cu²⁺, suggesting denaturation, nucleobase binding and aggregation of FS-DNA with Cu²⁺. Interestingly, here we observed hypochromicity with Mg²⁺, indicating folding and greater stabilization of FS-DNA with Mg²⁺, which reflects in higher phoretic drift of FS-DNA in gradient of Mg²⁺.

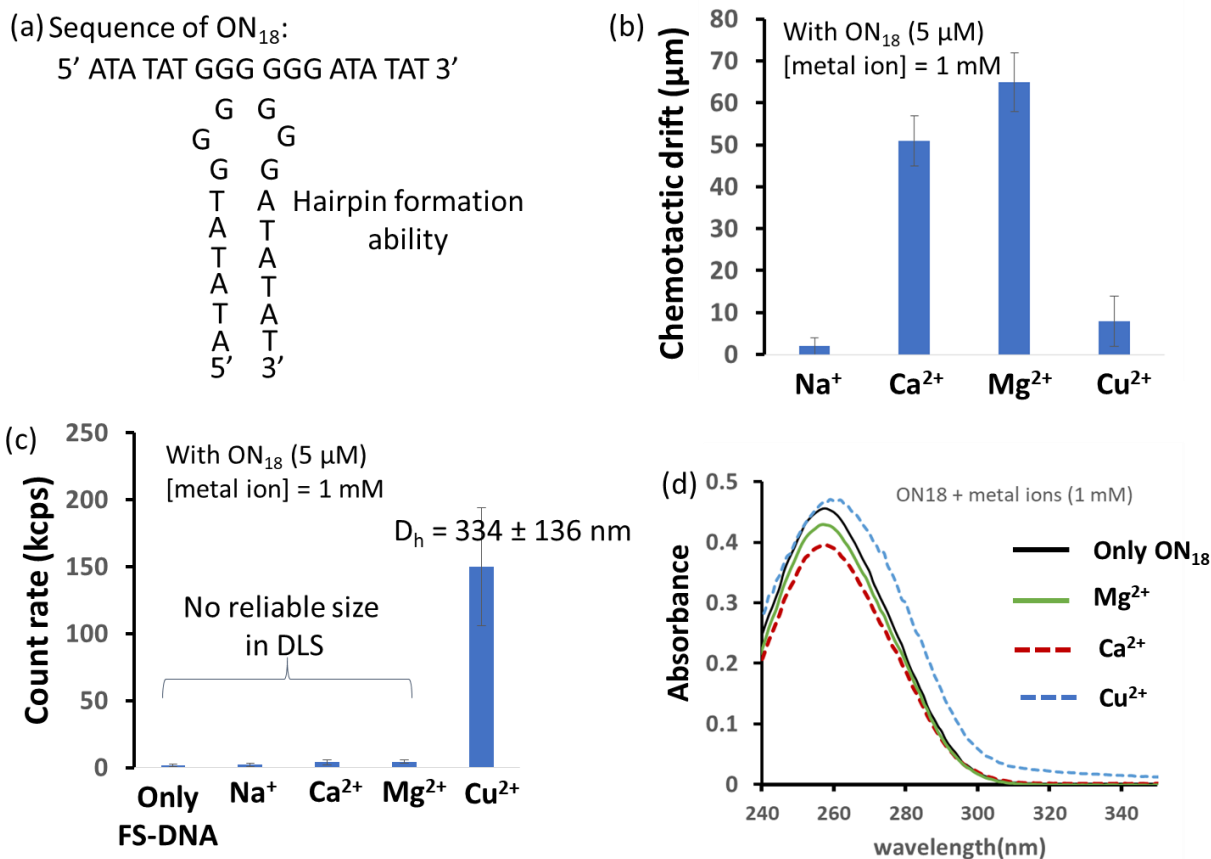


Fig. S13. (a) Sequence of the oligonucleotide and its hairpin formation ability and pattern. (b) Measured drift of ON₁₈ based on fluorescence intensity calculation towards metal ion side in the experimental set up as denoted in Fig. 3a and S8. Here, fixed concentration (1 mM) of Na⁺, Mg²⁺, Ca²⁺ or Cu²⁺ with NO₃⁻ as counter ion passed through the bottom inlet and ON₁₈ with AO through top. (b) Count rate (kcps) of ON₁₈ in presence of different metal ions (1 mM) and [ON₁₈] = 5 μM, obtained from DLS measurement. Except Cu²⁺, in all other cases, count rate remains low. It suggests only in presence of Cu²⁺, detectable colloidal aggregate was observed for ON₁₈, which also suggests decreasing of diffusion coefficient of smaller sized FS-DNA in presence of Cu²⁺. (c) UV-vis absorbance spectra of ON₁₈ in absence and presence of metal ions. Here also hyperchromicity and a red-shift of 3 nm of ON₁₈ absorbance maxima was observed in case of Cu²⁺, suggesting nucleobase binding and aggregation of ON₁₈ with Cu²⁺. Interestingly, here we observed hypochromicity with Mg²⁺ and Ca²⁺ indicating folding and greater stabilization of ON₁₈ and higher phoretic drift.

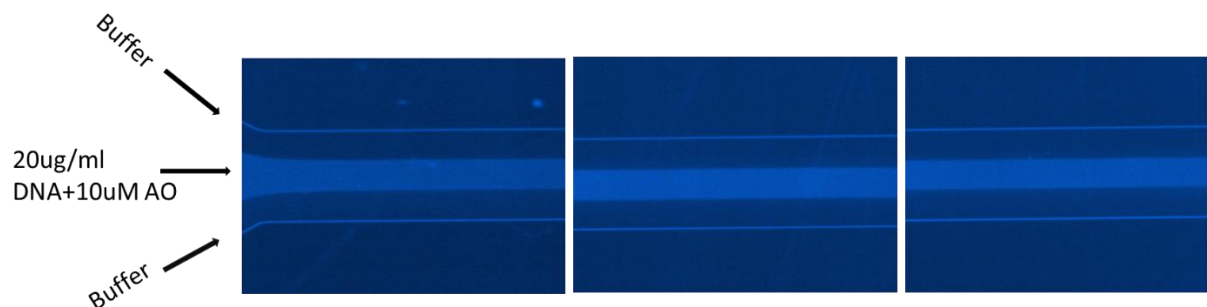


Fig. S14. Representative fluorescence microscopic images of 3-inlet and 1-outlet of the microfluidics channel with a flow rate of 0.1ml/hr where 20 μ g/ml CT-DNA and 10 μ M of AO was injected from the middle inlet and aqueous buffer from the top and the bottom inlet.

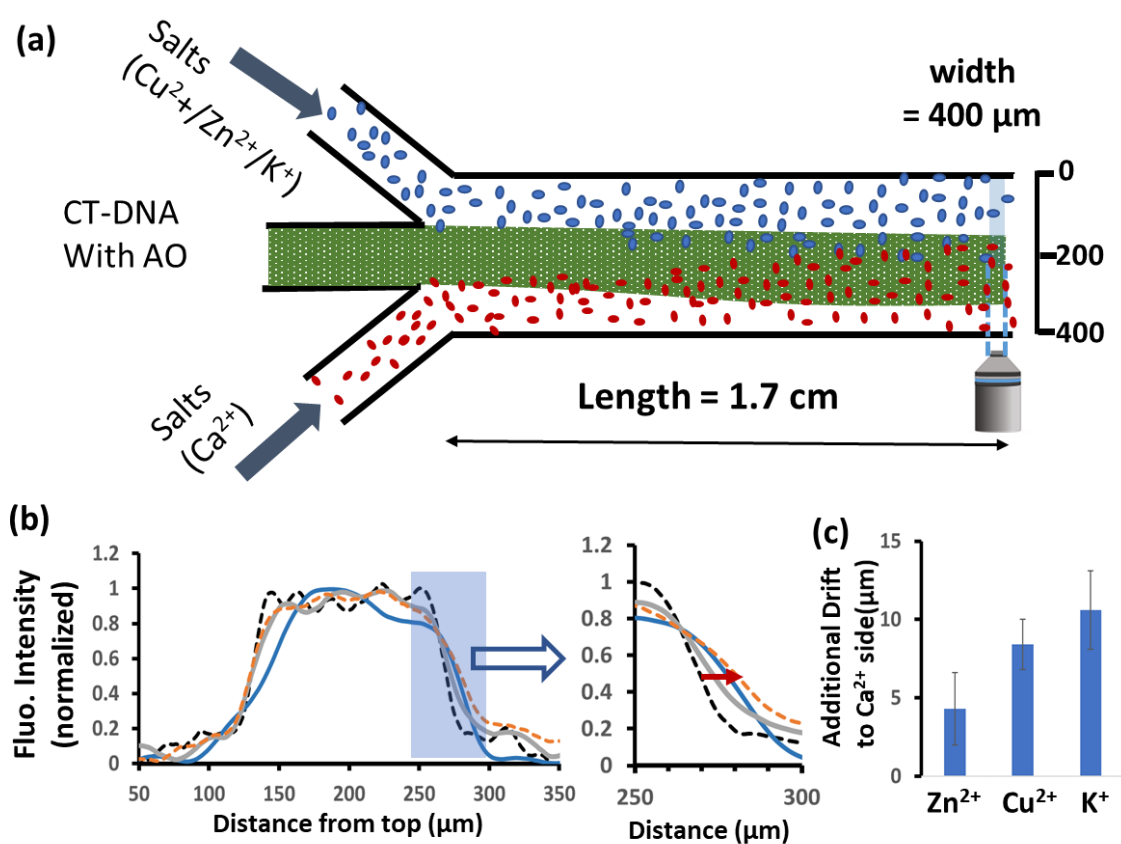


Fig. S15. (a) Schematic of the 3-inlet set up where from the middle inlet CT-DNA was injected and from bottom Ca^{2+} ion and through top either Cu^{2+} or Zn^{2+} or K^+ ion containing aqueous solution; (b-c) Representative fluorescence intensity profile of outlet; (d) Measured drift of CT-DNA towards Ca^{2+} side when Zn^{2+} or Cu^{2+} or K^+ are in the opposite side compared to no salt condition. Flow speed = 0.3 ml/hr. [CT-DNA] = 20 μ g/ml, [metal ion] = 1 mM, [AO] = 10 μ M.

Here we performed microfluidic experiment in a competing metal ion gradient environment. We passed CT-DNA with AO and Ca^{2+} through middle and bottom channel, respectively ($\text{Re} = 0.32$, laminar flow). Herein, through top inlet we passed either salt of Cu^{2+} or Zn^{2+} or K^+ -salt solution (1 mM) (Fig. S14-S15, ESI). We chose these experimental condition as from our previous experiment we found Ca^{2+} led to highest drift and the other ions were on the bottom side. Next we measured the fluorescence intensity near the outlet in each cases and found fluorescence intensity drifted towards Ca^{2+} ion side. In fact, we found the maximum drift is for $\text{K}^+ > \text{Cu}^{2+} > \text{Zn}^{2+}$. Overall, this study suggest that CT-DNA tends to move towards the metal ion, where it is stable, binds strongly but with the phosphate backbone and also retains its native diffusion co-efficient.

H. Theoretical modeling for chemotactic drift

To understand the migratory behavior of DNA-metal complex when coordinated with DNA, we modeled an electrophoresis device having one inlet and one outlet (length = 17 mm, width = 0.6 mm) using COMSOL Multiphysics (5.6 version) (Fig. S16). (see also ref. 12 of the main manuscript) This model uses electrophoretic transport and the laminar flow interfaces / modules. A laminar carrier stream of DNA -metal was injected through inlet with 0.3 ml/h fluid velocity and the components were separated by migratory transport in an electric field. The electrophoretic transport module connects transport of ionic species by diffusion, convection, and migration in electric fields. The mass-balance equation used here to solve the DNA-metal migration is as follows:

$$\nabla \cdot (-D_i \nabla c_i - z_i u_{m,i} F c_i \nabla V) + u \cdot \nabla c_i = 0 \quad (\text{S1})$$

where c_i be the concentration of species, D_i be the diffusion coefficient of i^{th} species, u denotes the fluid velocity, F be the Faraday's constant, V be the electric potential, z_i denotes the charge number of ionic species, and $u_{m,i}$ denotes the ionic mobility of species.

Apart from this, we also used equations for the charge transport in the electrolyte by assuming electroneutrality condition, and a set of chemical equilibria for water self-ionization and dissociation reactions of weak acids and weak bases incorporated in the Electrophoretic module of COMSOL. The fluid flow set up includes solving of Navier-Stokes equations along with Laminar flow.

For parameters, here we considered the bottom wall of channel as having negative potential (-50 mV) equal to zeta potential of DNA, while top wall having no potential. Then we injected DNA-metal species (1 mM) from inlet along with weak acid ($\text{pK}_a = 7$, mobility = 2.4×10^{-13} s.mol/Kg) and weak base ($\text{pK}_a = 7$, mobility = 2.4×10^{-13} s.mol/Kg) to maintain neutrality. The isoelectric point used for DNA-metal species is 2.^{S1} The experimentally observed diffusion

coefficient of DNA-metal species used in solving above equations are given in Table S2. We wanted to check here how much DNA along with DNA-metal ion conjugate which is at the center of the channel moved towards or away from the metal ion side. On simulating this system, we observed shift of DNA-metal ion conjugated species towards top wall of channel, that is towards metal ion. The order of shifting of DNA-metal species was maximum for Ca^{2+} and minimum for Cu^{2+} . Herein, we have observed some amount of drift for Na^+ and K^+ ions also, which was higher than Cu^{2+} in contrary to the experiment. However, we believe in case of experiment the amount of formed DNA- Na^+ and DNA- K^+ complex is much lower due to their low binding affinity (3-4 order of magnitude lower than divalent ions), which has not been considered in the theoretical study (Table S1).

Outlet images of Cu^{2+} and Ca^{2+} is shown in Fig. S17.

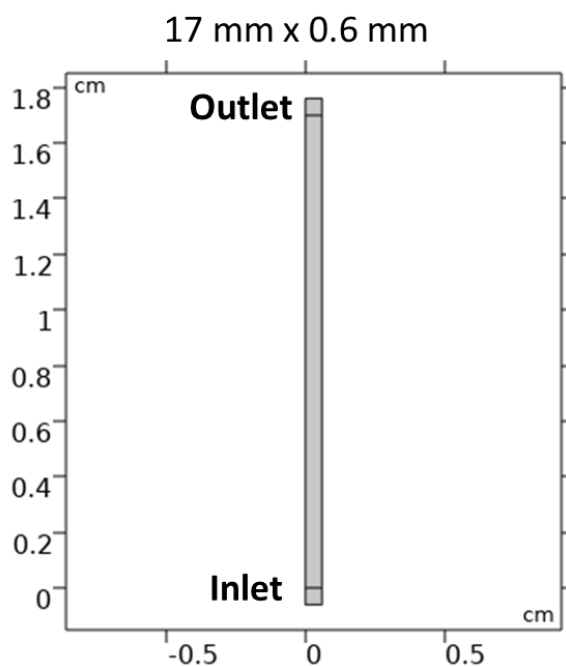


Fig. S16. Schematic representation of one inlet-one one-outlet chip.

Table S2. Experimentally observed diffusion coefficient of DNA and DNA-metal conjugate. Experimental condition: $[\text{CT-DNA}] = 50 \mu\text{g/ml}$; $[\text{salt}] = 1 \text{ mM}$; $\text{pH} = 7$, Tris buffer (5 mM).

Species	Diffusion Coefficient (cm^2/s)
DNA- Na^+	2.1×10^{-8}

DNA-K ⁺	2.5×10^{-8}
DNA-Ca ²⁺	6.6×10^{-8}
DNA-Mg ²⁺	6×10^{-8}
DNA-Cu ²⁺	3.5×10^{-9}
DNA-Zn ²⁺	4.3×10^{-8}
DNA	3×10^{-8}

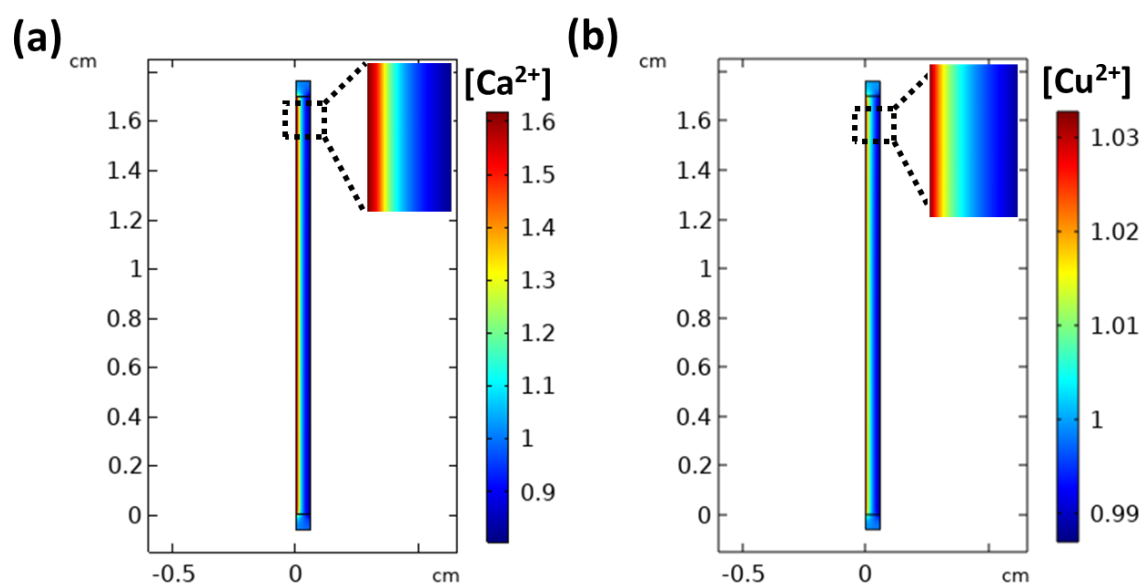


Fig. S17. Outlet images of shift in DNA-metal species (DNA-Ca²⁺ and DNA-Cu²⁺).

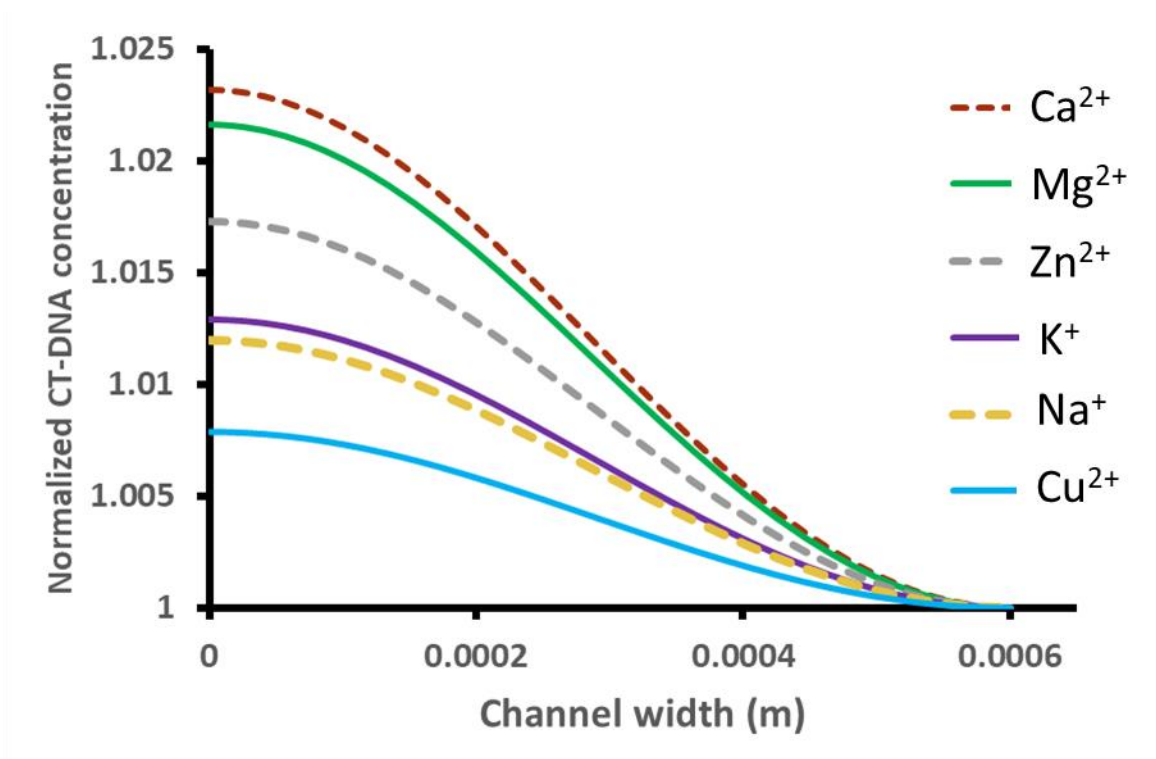


Fig. S18. Normalized concentration distribution of [DNA-metal conjugate] + [DNA] along the channel width, achieved after simulation through COMSOL.

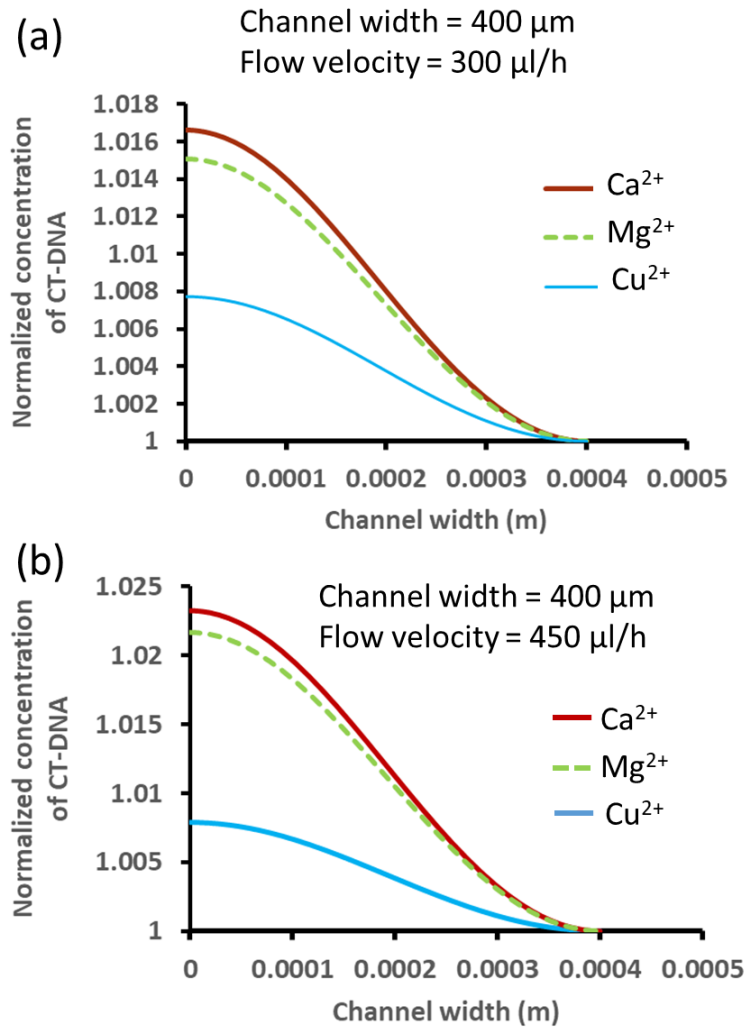


Fig. S19. Normalized concentration distribution of [DNA-metal conjugate] + [DNA] along the channel width in a channel width of 0.4 mm with flow velocity of (a) 300 $\mu\text{l/h}$ and (b) 450 $\mu\text{l/h}$, achieved after simulation through COMSOL.

The data obtained from Fig. S18 and S19 indicates, the pattern of the drift with respect to different ions remain similar irrespective of the magnitude of flow velocity and channel width. The pecllet number (Advective transport rate/Diffusive transport rate) of the flow which depends on the (channel width \times flow velocity) remains identical for the situation in case Fig. 18 and Fig. S19b and thus it showed similar drift behavior. Thus, in case of 3-inlet channel, although the channel width is smaller, the magnitude of phoretic drift will be decreased a bit, as similar flow velocity (0.3 ml/h) through the channel has been used. To get the similar extent of phoretic drift behavior through different width of channel under laminar flow condition, the pecllet number needs to be kept at a constant value by modulating the flow velocity.

I. Coffee ring effect

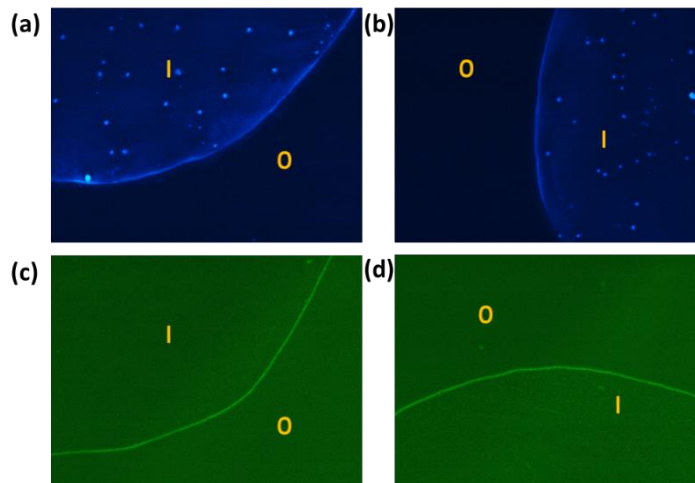


Fig. S20: Fluorescent Microscopic Images of spatiotemporal pattern of the ring-like structure formation after evaporation of the droplet consisting CT-DNA (a)&(b) with AO (acridine orange) and (c)&(d) with fluorescent carboxylate beads Experimental Condition: [CT-DNA]= 20 $\mu\text{g/ml}$, [AO]= 10 μM , [Fluorescent carboxylate bead 1 μm]= 0.025 % , [Tris-HCl buffer pH 7]= 5mM at 25°C. Here I: Inside drop O: Outside drop. X-axis of each image= 1.6 mm.

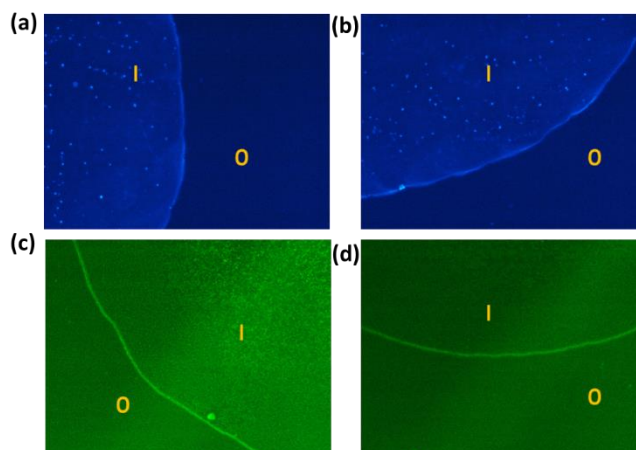


Fig. S21: Fluorescent Microscopic Images of spatiotemporal pattern of the ring-like structure formation after evaporation of the droplet consisting CT-DNA uniformly mixed with Ca^{2+} (a)&(b) with AO (acridine orange) and (c)&(d) with fluorescent carboxylate beads Experimental Condition: [CT-DNA]= 20 $\mu\text{g/ml}$, [Ca^{2+}]= 1mM, [AO]= 10 μM , [Fluorescent carboxylate bead 1 μm]= 0.025 % , [Tris-HCl buffer pH 7]= 5mM at 25°C. Here I: Inside drop O: Outside drop. X-axis of each image= 1.6 mm.

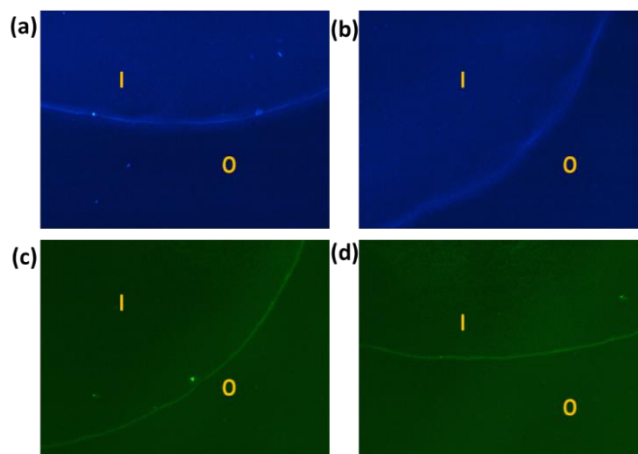


Fig. S22. Fluorescent Microscopic Images of spatiotemporal pattern of the ring-like structure formation after evaporation of the droplet consisting CT-DNA uniformly mixed with Cu^{2+} and Ca^{2+} (a)&(b) with AO (acridine orange) and (c)&(d) with fluorescent carboxylate beads. Experimental Condition: $[\text{CT-DNA}] = 20 \mu\text{g/ml}$, $[\text{Ca}^{2+}] = 0.9\text{mM}$, $[\text{Cu}^{2+}] = 0.1\text{mM}$, $[\text{AO}] = 10 \mu\text{M}$, $[\text{Fluorescent carboxylate bead } 1 \mu\text{m}] = 0.025 \%$, $[\text{Tris-HCl buffer pH } 7] = 5\text{mM}$ at 25°C . Here I: Inside drop O: Outside drop. X-axis of each image=1.6 mm.

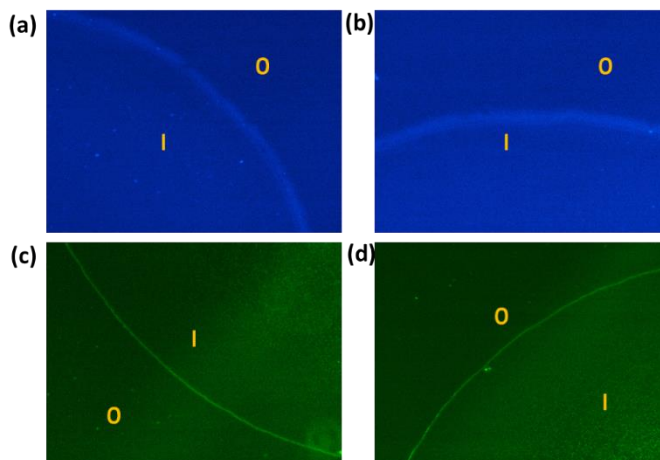


Fig. S23. Fluorescent Microscopic Images of spatiotemporal pattern of the ring-like structure formation after evaporation of the droplet consisting CT-DNA uniformly mixed with Cu^{2+} and Ca^{2+} (a)&(b) with AO (acridine orange) and (c)&(d) with fluorescent carboxylate beads. Experimental Condition: $[\text{CT-DNA}] = 20 \mu\text{g/ml}$, $[\text{Ca}^{2+}] = 0.7\text{mM}$, $[\text{Cu}^{2+}] = 0.3\text{mM}$, $[\text{AO}] = 10 \mu\text{M}$, $[\text{Fluorescent carboxylate bead } 1 \mu\text{m}] = 0.025 \%$, $[\text{Tris-HCl buffer pH } 7] = 5\text{mM}$ at 25°C . Here I: Inside drop O: Outside drop. X-axis of each image= 1.6 mm.

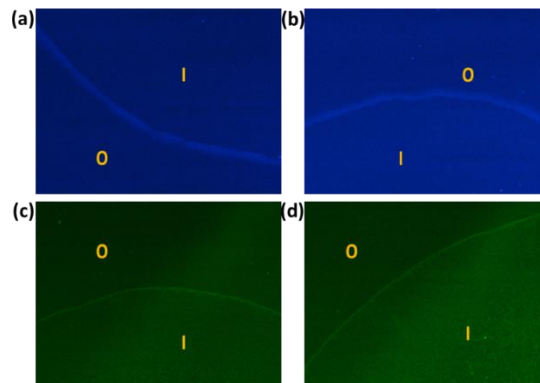


Fig. S24. Fluorescent Microscopic Images of spatiotemporal pattern of the ring-like structure formation after evaporation of the droplet consisting CT-DNA uniformly mixed with Cu^{2+} and Ca^{2+} (a)&(b) with AO (acridine orange) and (c)&(d) with fluorescent carboxylate beads. Experimental Condition: $[\text{CT-DNA}] = 20 \mu\text{g/ml}$, $[\text{Ca}^{2+}] = 0.5\text{mM}$, $[\text{Cu}^{2+}] = 0.5\text{mM}$, $[\text{AO}] = 10 \mu\text{M}$, $[\text{Fluorescent carboxylate bead } 1 \mu\text{m}] = 0.025 \%$, $[\text{Tris-HCl buffer pH } 7] = 5\text{mM}$ at 25°C . Here I: Inside drop O: Outside drop. X-axis of each image= 1.6 mm.

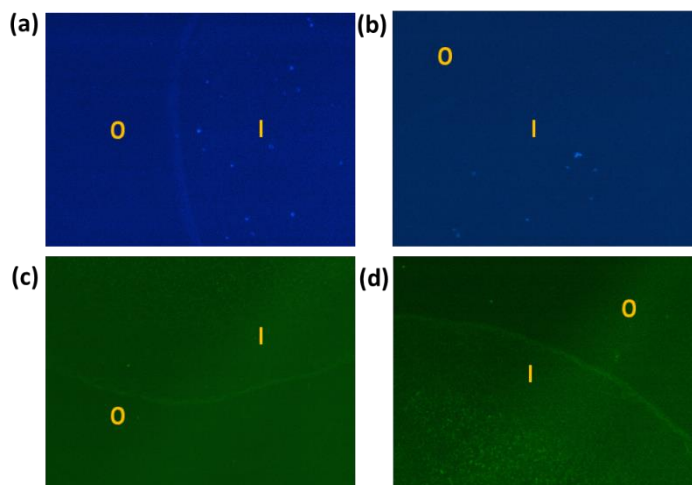


Fig. S25. Fluorescent Microscopic Images of spatiotemporal pattern of the ring-like structure formation after evaporation of the droplet consisting CT-DNA uniformly mixed with Cu^{2+} and Ca^{2+} (a)&(b) with AO (acridine orange) and (c)&(d) with fluorescent carboxylate beads. Experimental Condition: $[\text{CT-DNA}] = 20 \mu\text{g/ml}$, $[\text{Ca}^{2+}] = 0.3\text{mM}$, $[\text{Cu}^{2+}] = 0.7\text{mM}$, $[\text{AO}] = 10 \mu\text{M}$, $[\text{Fluorescent carboxylate bead } 1 \mu\text{m}] = 0.025 \%$, $[\text{Tris-HCl buffer pH } 7] = 5\text{mM}$ at 25°C . Here I: Inside drop O: Outside drop. X-axis of each image= 1.6 mm.

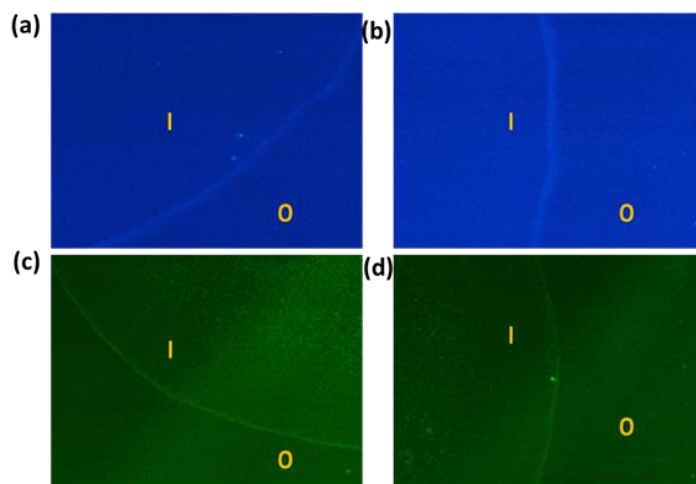


Fig. S26. Fluorescent Microscopic Images of spatiotemporal pattern of the ring-like structure formation after evaporation of the droplet consisting CT-DNA uniformly mixed with Cu^{2+} and Ca^{2+} (a)&(b) with AO (acridine orange) and (c)&(d) with fluorescent carboxylate beads. Experimental Condition: $[\text{CT-DNA}] = 20 \mu\text{g/ml}$, $[\text{Ca}^{2+}] = 0.1\text{mM}$, $[\text{Cu}^{2+}] = 0.9\text{mM}$, $[\text{AO}] = 10 \mu\text{M}$, $[\text{Fluorescent carboxylate bead } 1 \mu\text{m}] = 0.025 \%$, $[\text{Tris-HCl buffer pH } 7] = 5\text{mM}$ at 25°C . Here I: Inside drop O: Outside drop. X-axis of each image = 1.6 mm.

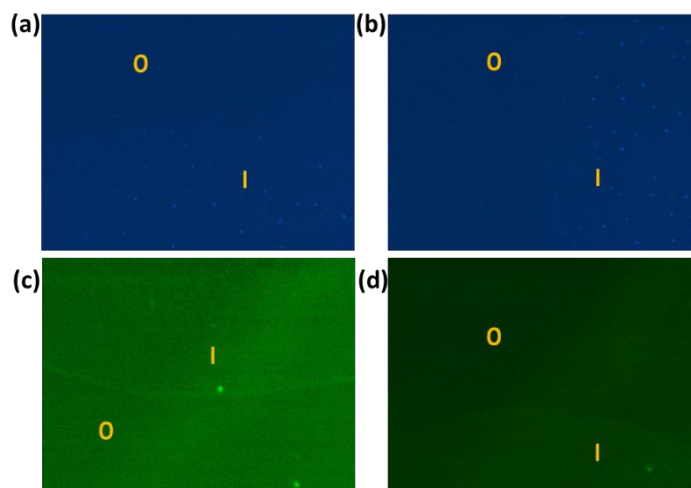


Fig. S27. Fluorescent Microscopic Images of spatiotemporal pattern of the ring-like structure formation after evaporation of the droplet consisting CT-DNA uniformly mixed with Cu^{2+} (a)&(b) with AO (acridine orange) and (c)&(d) with fluorescent carboxylate beads. Experimental Condition: $[\text{CT-DNA}] = 20 \mu\text{g/ml}$, $[\text{Cu}^{2+}] = 1 \text{mM}$, $[\text{AO}] = 10 \mu\text{M}$, $[\text{Fluorescent carboxylate bead } 1 \mu\text{m}] = 0.025 \%$, $[\text{Tris-HCl buffer pH } 7] = 5\text{mM}$ at 25°C . Here I: Inside drop O: Outside drop. X-axis of each image = 1.6 mm.

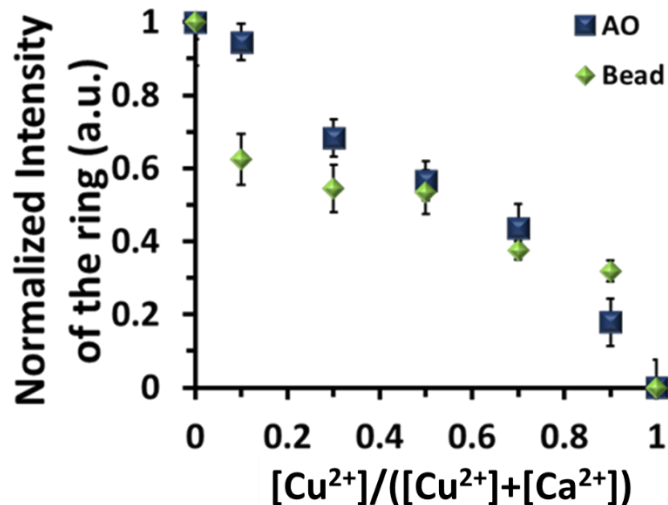


Fig. S28: Normalized Fluorescence intensity of spatiotemporal pattern of the ring-like structure formation after evaporation of the droplet consisting CT-DNA uniformly mixed with Cu^{2+} and Ca^{2+} . Experimental Condition: [CT-DNA] = 20 μ g/ml, [AO]= 10 μ M, [Fluorescent carboxylate bead 1 μ m] = 0.025 % , [Tris-HCl buffer pH 7]= 5mM at 25°C. Total salt concentration = 1 mM.

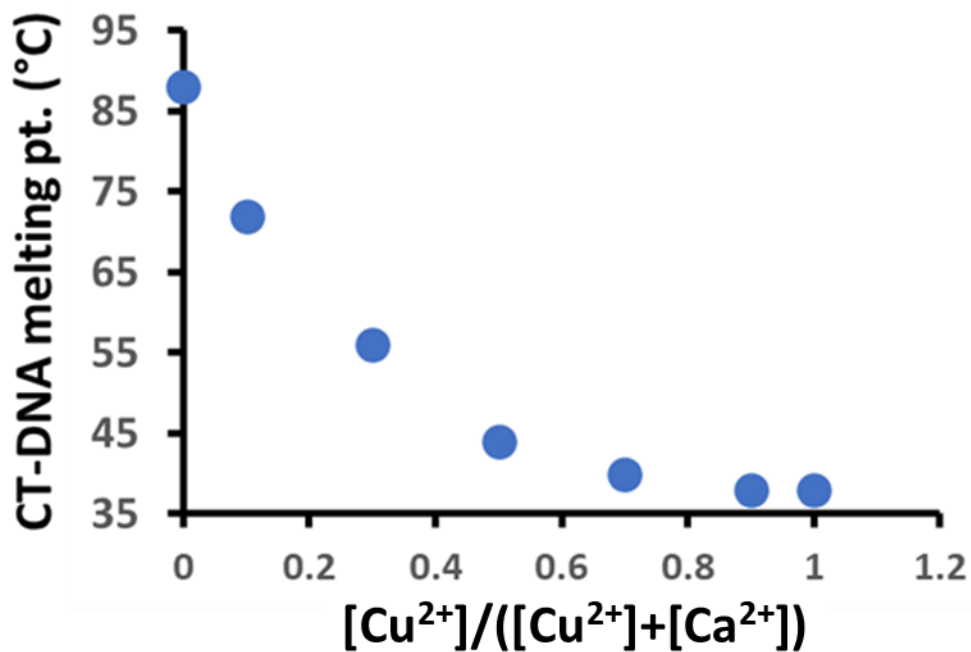


Fig. S29. Melting temp of CT-DNA uniformly mixed with Cu^{2+} and Ca^{2+} at different ratio. Experimental Condition: [CT-DNA] = 20 μ g/ml, [AO]= 10 μ M, [Fluorescent carboxylate bead 1 μ m] = 0.025 % , [Tris-HCl buffer pH 7]= 5mM at 25°C. Total salt concentration = 1 mM.

Upon comparing Fig. S28 and S29, a striking similarity with their ring formation propensity and melting point behavior has been observed. With increasing Cu^{2+} , m.pt. of CT-DNA or native stability of CT-DNA decreased (m.pt. of native CT-DNA in absence of any metal ion is 65 °C) and thereby we also observed lesser ring formation ability of CT-DNA droplet upon evaporation (both in presence of intercalator AO and fluorescent microbead). Thus, here by modulating DNA stability by means of content of metal ions (mixture of DNA stabilizing, Ca^{2+} and denaturing Cu^{2+}), the nature of coffee ring pattern can be modulated.

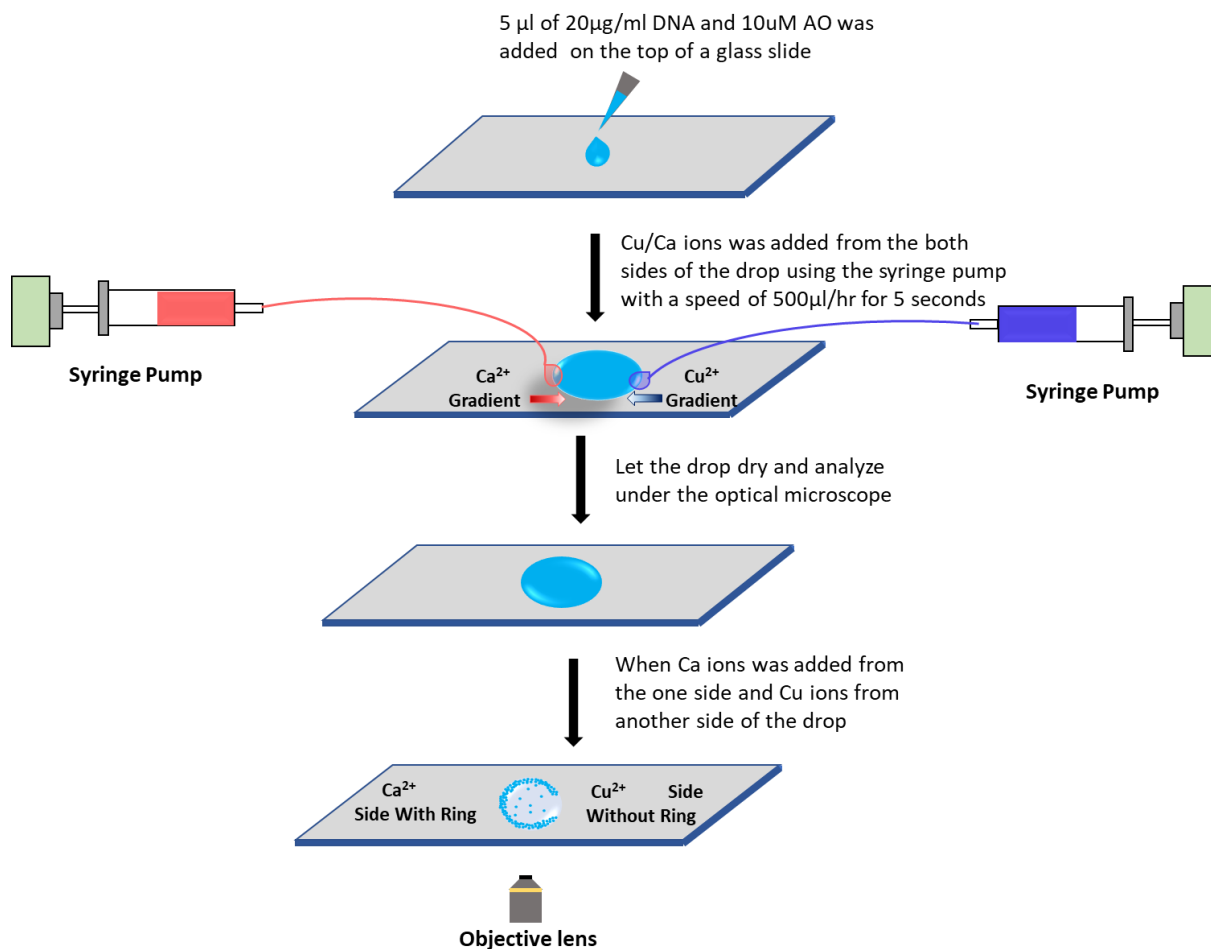


Fig. S30. Schematic representation of the experimental setup for the spatiotemporal pattern of ring-like structure formation when metal ions were added from opposite sides of the droplet.

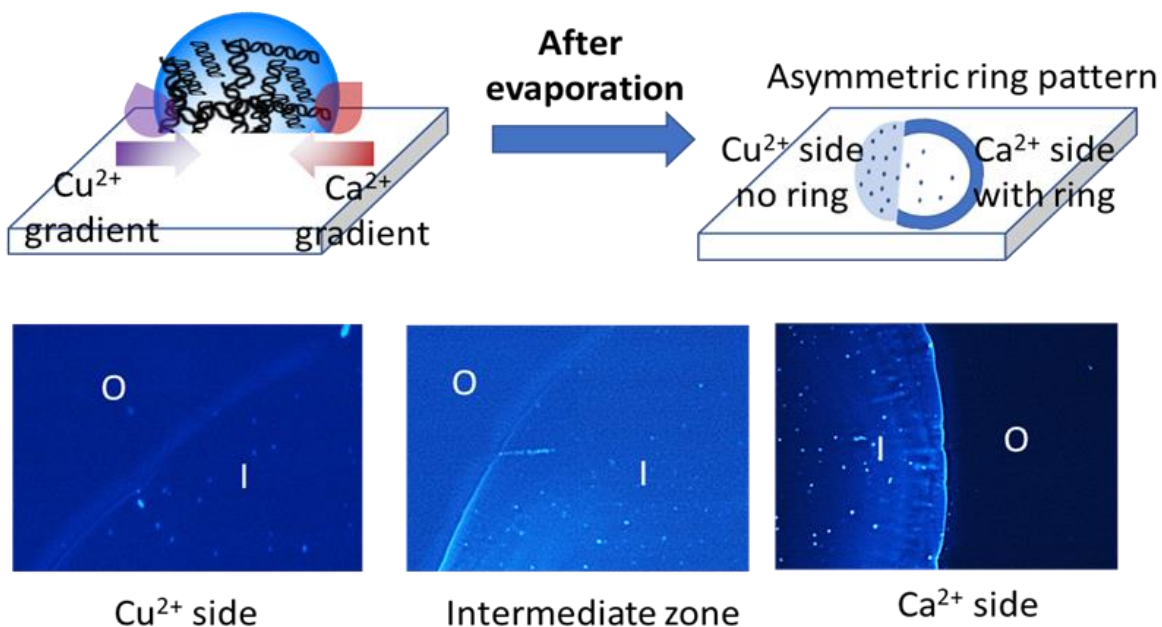


Fig. S31. Fluorescence microscopic images of spatiotemporal pattern of the ring-like structure formation after evaporation of the droplet consisting CT-DNA when Ca²⁺ and Cu²⁺ salt were added in two opposite sides of the droplet. Experimental condition: [CT-DNA] = 20 $\mu\text{g/ml}$, [AO] = 10 μM . X-axis for each image is 1.6 mm.

Overall, we showed the ability to simultaneously generate both uniform and non-uniformly coated DNA surface by judiciously choosing metal ions at our experimental condition.

Theoretical explanation of coffee ring formation behavior: Calculation of Capillary-phoresis Number (CP)

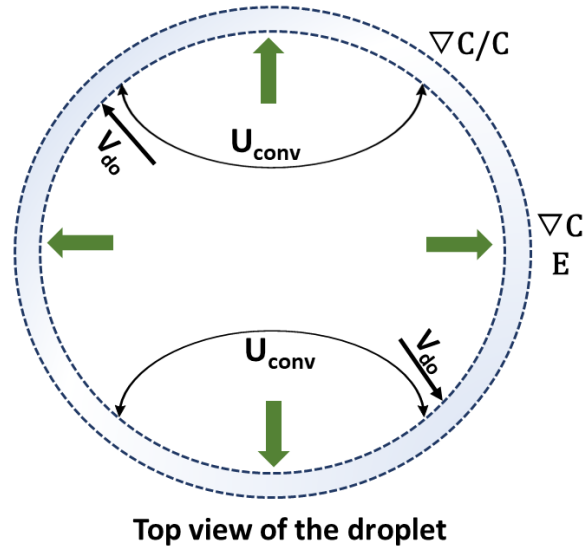


Figure S32. Schematic representation of top view of a droplet.

The Capillary-phoresis number (CP) is used to explain the observed dependence on salt system of DNA coffee-ring patterns and measured as discussed in reference S3 and S4 and ref. 9 of the main manuscript.

$$CP = \frac{U_{el}}{U_{conv}} \quad \dots\dots\dots S2$$

where, U_{el} is the net electrokinetic velocity which is a combination of particle diffusiophoretic (U_{dp}) and fluid diffusion-osmotic velocities (V_{do}), U_{conv} is the velocity due to fluid capillary convection.

$$U_{el} = \frac{\epsilon k T}{\eta_v z e R} \beta (\zeta_p - \zeta_w) \frac{\nabla C_{ali}(\eta)}{C_{ali}(\eta)} \quad \dots\dots\dots S3$$

where, β is a dimensionless diffusivity parameter for a binary symmetric electrolyte and β is expressed as:

$$\beta = \frac{D_+ - D_-}{D_+ + D_-} \quad \dots\dots\dots S4$$

On rearranging the equation of U_{el} and U_{conv} , we get

$$CP = \frac{\varepsilon k T t_e}{\eta_v Z e R^2} \beta (\zeta_p - \zeta_w) \quad \dots\dots\dots S5$$

where, $U_{conv} \sim R/t_e$, $\nabla C_{dii}(\eta)/C_{dii}(\eta) \sim 1/R$ and $\frac{\varepsilon k T t_e}{\eta_v Z e R^2} = K$

$$\text{So, } CP = K \beta (\zeta_p - \zeta_w) \quad \dots\dots\dots S6$$

where, $K = -0.0076$

for Ca^{2+} : $\beta = -0.41$, $\zeta_p = -26.56$, $\zeta_w = -30.75$, $CP = 0.013$
 & for Cu^{2+} : $\beta = -0.45$, $\zeta_p = -16.06$, $\zeta_w = -6.07$, $CP = -0.034$

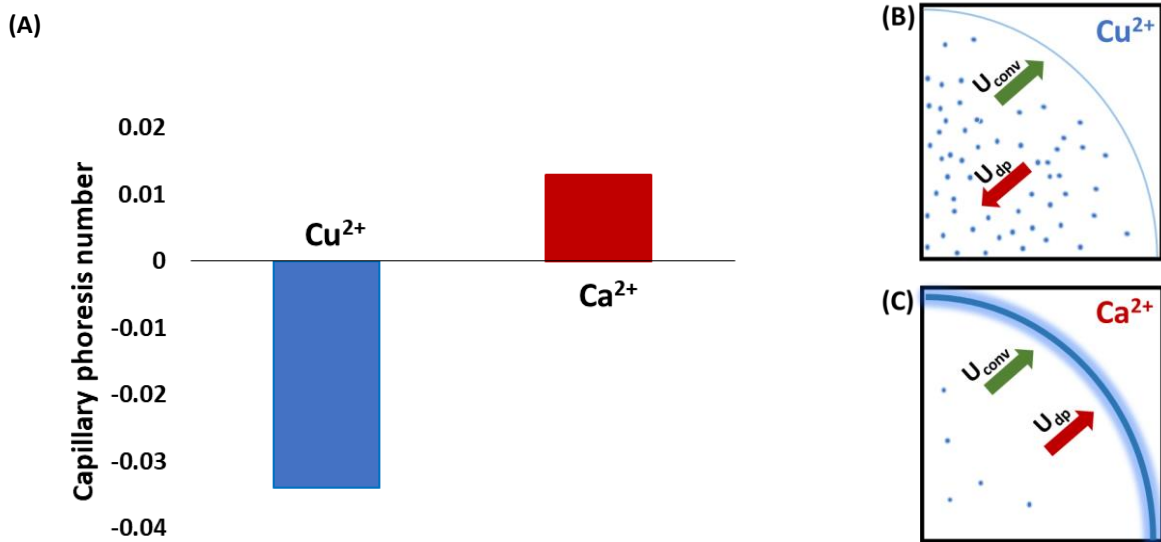


Fig. S33: (A) Graphical representation of calculated capillary phoresis number (B) In case of Cu²⁺, U_{conv} and U_{dp} are in the opposite direction (C) In case of Ca²⁺, U_{conv} and U_{dp} are in the same direction.

The value of parameter used to calculate Capillary-phoresis number (CP) are as follows:

$D_{Ca^{2+}} = 0.7920 \times 10^5 \text{ cm}^2\text{s}^{-1}$, $D_{Cu^{2+}} = 0.7200 \times 10^5 \text{ cm}^2\text{s}^{-1}$, $D_{NO^3} = 1.9020 \times 10^5 \text{ cm}^2\text{s}^{-1}$ are the diffusivity of the ions.^{S5}

R = 2 mm, radius of the drop.

t_e = 30 min(approx.), evaporation time of the drop (as per our experimental observation)

ε denotes the dielectric permittivity of the water

ζ_w is the wall or substrate surface zeta potential

$\eta = 0.89 \times 10^{-3} \text{ Pa}\cdot\text{s}$, viscosity of water

$T = 25 \text{ }^\circ\text{C}$, room temperature

The formation of particle patterns (banding/dispersion) is significantly influenced by diffusiophoresis and convection as explained in equation S2 to S6. In our study, we performed systematic experiments to investigate the pattern formation of DNA with carboxylate polystyrene latex beads and acridine orange in presence of Ca^{2+} and Cu^{2+} ions. The particles suspended in a droplet typically deposit in a ring-like pattern as it dries on a surface. The movement of the particles is caused by three factors: (i) capillary convection within the droplet (U_{conv}); (ii) fluid diffusio-osmotic transport along the substrate surface; and (iii) diffusiophoretic transport of the particles in the salt gradient (U_{dp}) in which U_{dp} and V_{do} affects by $\nabla C/C$ ratio. In our study we observed that in presence of Ca^{2+} ions, thicker and compact ring was observed but in presence of Cu^{2+} ions narrower and broken ring was observed. It infers that U_{conv} and U_{dp} are pointed in the same direction in case of Ca^{2+} ions while in case of Cu^{2+} ions they are pointed in opposite direction (Fig. S32). As mentioned, we calculated Capillary-phoresis number (CP) in case of both Ca^{2+} and Cu^{2+} (Fig. S33).

Herein, for $\text{Ca}(\text{NO}_3)_2$, the CP value of CT-DNA in our experimental condition was +ve and slightly greater than 0.01. In contrary, for $\text{Cu}(\text{NO}_3)_2$, this value was -ve with a value of -0.03. Now, higher the CP value, higher is the coffee ring pattern formation ability. Thus in case of Ca^{2+} , we observed distinct coffee ring pattern for CT-DNA, whereas for Cu^{2+} , it is not.

J. References:

- S1. Y. -A. Song, S. Hsu, A. L. Stevens and J. Han, *Anal. Chem.*, 2006, **78**, 3528-3536.
- S2. S. Yetgin and D. Balkose, *RSC Adv.*, 2015, **5**, 57950- 57959.
- S3. Á. G. Marín, H. Gelderblom, D. Lohse and J. H. Snoeijer, *Phys. Rev. Lett.*, 2011, **107**, 085502.
- S4. R. D. Deegan, O. Bakajin, T. F. Dupont, G. Huber, S. R. Nagel and T. A. Witten, *Nature*, 1997, **389**, 827–829.
- S5. Petr Vanýsek: Ionic conductivity and diffusion at infinite dilution, Handbook of Chemistry and Physics, CRC Press, 1992/93 edition. Boca Raton, 1992. pp. (5-111)-(5-113).